

Origin of the photoemission final-state effects in $\text{Bi}_2\text{Sr}_2\text{CaCu}_2\text{O}_8$ by very-low-energy electron diffraction

V. N. Strocov, R. Claessen

Experimentalphysik II, Universität Augsburg, D-86135 Augsburg, Germany

P. Blaha

Institut für Materialchemie, Technische Universität Wien, A-1060 Wien, Austria

(February 1, 2008)

Very-low-energy electron diffraction with a support of full-potential band calculations is used to achieve the energy positions, \mathbf{K}_{\parallel} dispersions, lifetimes and Fourier compositions of the photoemission final states in $\text{Bi}_2\text{Sr}_2\text{CaCu}_2\text{O}_8$ at low excitation energies. Highly structured final states explain the dramatic matrix element effects in photoemission. Intense $c(2\times 2)$ diffraction reveals a significant extrinsic contribution to the shadow Fermi surface. The final-state diffraction effects can be utilized to tune the photoemission experiment on specific valence states or Fermi surface replicas.

Photoemission (PE) spectra of $\text{Bi}_2\text{Sr}_2\text{CaCu}_2\text{O}_8$ ($\text{Bi}2212$) and other high-temperature superconductors can significantly deviate from the photohole spectral function $A(\mathbf{k}, \omega)$ due to an energy and \mathbf{k} dependence of the matrix element (ME) [1–4]. For example, the long debated dependence of the shape of the observed Fermi surface (FS) of $\text{Bi}2212$ on the photon energy $h\nu$ and experimental geometry has finally found its explanation in ME effects. A predictive use of these effects can help to resolve subtle details of the electronic structure of $\text{Bi}2212$ such as the bilayer splitting [2,3]. Presently, analysis of ME effects employs computational simulations of the PE process [1,2]. However, there remains an inherent uncertainty of a few eV due to the lack of any reliable knowledge about the energy location and lifetime of the PE final states. Additional complications are incommensurate (IC) structural modulations and antiferromagnetic (AFM) fluctuations, which manifest themselves in PE experiments, respectively, as diffraction replicas of the FS and so-called shadow FSs [5–7].

Very-Low-Energy Electron Diffraction (VLEED) gives direct access to the PE final states (see [8,9] and the references therein) based on the fact that, neglecting the electron-hole interaction within the sudden approximation, the PE final states are the time-reversed LEED states [10]. In the VLEED elastic electron reflectivity spectra $R(E)$, the energies of the spectral structures give the final-state dispersions $E(\mathbf{k})$, and their broadening the corresponding lifetimes τ expressed by the imaginary part $\text{Im } \Sigma$ of the self-energy as $\hbar/\tau = 2 \text{Im } \Sigma$.

We here use VLEED to achieve first direct information

on the PE final states in $\text{Bi}2212$ up to 45 eV above the Fermi level E_F and elucidate its immediate implications for the PE experiment.

Experiment and band calculations – The VLEED experiment was carried out using a standard LEED setup operated in the retarding field mode [9,11]. The total $R(E)$ integrated over all diffracted beams (plus structureless inelastic reflectivity) was measured in the target current $T(E)$. Intensities of individual beams were measured on the LEED screen using a CCD camera. Three samples with an oxygen content near optimal doping showed identical results.

The band calculations employed the full-potential APW+local orbitals method as implemented in the WIEN2k package [12]. The generalized gradient approximation (GGA) was used to describe exchange-correlation within the density functional theory (DFT). The calculations employed the body-centered-tetragonal (bct) crystal structure and a basis of 2200 augmented plane waves. The obtained $E(\mathbf{k})$, characterizing essentially the bulk states with infinite lifetime, was connected to the VLEED process based on Fourier expansion of the Bloch waves, which was used to evaluate the partial currents $T_{\mathbf{k}}$ into the crystal excited in each Bloch wave, and the integral $T(E)$ spectra [15]. Finite electron lifetime was simulated by Lorentzian smoothing and damping of $T(E)$ [8].

The experimental structural parameters from [13] and [14] were tested in the calculations, with the latters yielding the best agreement with the VLEED experiment. While the valence bands changed insignificantly, the unoccupied $E(\mathbf{k})$ was strongly sensitive to the structural parameters. Such a sensitivity suggests that any model of the final states, used in PE simulations, needs to be checked against the VLEED experiment.

Integral $T(E)$ spectra: Dispersions and lifetimes of the final states – The structures in $T(E)$ all reflect those in elastic $R(E)$, with the inelastic reflectivity giving only a featureless background. We start with analysis of the normal incidence spectrum in Fig.1(a). It corresponds, by parallel momentum conservation and assuming insignificant umklapp contributions from the IC superstructure, to the ΓZ direction of the Brillouin zone (BZ). A slope of $T(E)$ towards higher energies is due to an increase of the inelastic reflection. Its unusual steepness may indicate strong electron coupling in the cascade re-

laxation process. To emphasize the $T(E)$ structures, we subtracted a quadratic background, Fig.1(b).

The calculated $T(E)$ spectrum (minus a quadratic background) is also shown in Fig.1(b). A reasonable agreement with the experiment, especially considering the neglect of umklapp, confirms our theoretical model of the unoccupied states. The best overall agreement is achieved by shifting the calculations by ~ 3 eV to higher energies. Besides the computational approximations, this can be attributed to excited-state self-energy corrections $\Delta\Sigma$ to the DFT-GGA exchange-correlation. The experiment suggests certain band dependence of $\Delta\Sigma$.

Guided by the calculated $T(E)$, we can trace the band structure origin of the experimental $T(E)$ structures. The $T(E)$ maxima are seen to reflect manifolds of so-called coupling bands (= dominant final states in PE) which are characterized by large partial $T_{\mathbf{k}}$ currents [9,15]. The $T(E)$ minima reflect the gaps between such manifolds. Individual bands are however not resolved in $T(E)$ because their energy separation is much smaller than $\text{Im}\Sigma$. Note that the coupling bands, apart from effective coupling to the incident plane wave, must have a 3-dimensional (3D) character with considerable k_{\perp} dispersion to transmit current into the crystal; they originate from the electronic orbitals oriented off-plane. The 2-dimensional (2D) bands, originating from the in-plane orbitals, are ineffective in both VLEED and PE.

Finite electron lifetime manifests itself in broadening and damping of the $T(E)$ structures. We estimated the energy dependence of $\text{Im}\Sigma$ based on its approximate parametric relation to the dielectric function ϵ as $\text{Im}\Sigma(E) = a + b \int_0^E \text{Im}[-1/\epsilon(\mathbf{q} = 0, \omega)] d\omega$ with $\epsilon(\mathbf{q} = 0, \omega)$ taken from the electron energy loss data [16]. The parameters a and b were optimized to bring the calculated $T(E)$ to the best agreement with the experiment in broadening and damping of the spectral structures. The obtained $\text{Im}\Sigma(E)$, which yields the calculated $T(E)$ in Fig.1 (b), is shown in the insert in Fig.1 (a) superimposed on $\epsilon(\mathbf{q} = 0, \omega)$. The increase of $\text{Im}\Sigma$ results from two plasmon peaks in $\epsilon(\mathbf{q} = 0, \omega)$ associated with the CuO valence bands [16]. This increase of $\text{Im}\Sigma$ in the final states explains, for example, why the PE intensity ratio of the CuO bilayer bonding and antibonding states varies with $h\nu$ above 30 eV much smoother in the experiment than in simulations employing constant $\text{Im}\Sigma = 1$ eV [17] relevant closer to $h\nu$ of 20 eV.

Based on the experimental $\text{Im}\Sigma(E)$ and calculated band dispersions, we found that the inelastic electron scattering limits the mean free path λ around 3 Å, decreasing with energy, in agreement with the electron energy loss data [16]. In the final-state band gaps λ is further reduced by elastic scattering off the crystal potential, resulting in a diffraction structure in $\lambda(E)$, particularly strong where $\text{Im}\Sigma$ is small. Qualitatively, it follows the structure in $T(E)$ where the maxima reveal the 3D states

enabling effective electron transport (accurate evaluation of λ involves calculations of damped Bloch waves [9,11]). Predictive tuning λ based on the experimental $T(E)$ can therefore be employed in the PE experiment to resolve signals from different atomic layers.

Experimental dispersion of the $T(E)$ spectra with the incidence \mathbf{K}_{\parallel} varying in the ΓX azimuth (perpendicular to the IC superstructure) is shown in Fig.2 (left). The shading shows the energy intervals of the $T(E)$ maxima reflecting the coupling bands. This map gives therefore the surface-projected \mathbf{K}_{\parallel} dispersions of the final states.

Our VLEED results give the first direct evidence of unoccupied quasiparticle dispersions in Bi2212, whereas the inverse PE studies near E_F (see, e.g., [18]) found only dispersionless states. Furthermore, the highly structured non-parabolic dispersions illustrate a general fact that at low excitation energies the final states, especially for complex materials, dramatically deviate from a free-electron-like continuum due to multiple scattering on the crystal potential. This property of the final states is the essential origin of dramatic $h\nu$ dependences in PE.

The results for the ΓY azimuth (along the IC superstructure) are shown in Fig.2 (right). By the fundamental lattice symmetry the ΓY azimuth is equivalent to ΓX , but this is complicated by the IC superstructure. The ΓY dispersion image can then be viewed as the ΓX dispersion with its IC umklapp replicas superimposed and hybridized with the main dispersion. The observed image resembles therefore a smeared ΓX dispersion.

The dispersion in ΓY comes at first glance as a surprise: Competing fundamental and IC potentials results in the collapse of strict periodicity (and the entire band structure concept) and thereby the parallel momentum conservation. As all states are now available for any incident \mathbf{K}_{\parallel} , one might expect that any dispersion in \mathbf{K}_{\parallel} would be lost. However, the VLEED spectra depend, apart from bare availability of the states, on how their wavefunctions match the incident plane wave [15]. Variation of the matching conditions with \mathbf{K}_{\parallel} results in the observed dispersion. A similar appearance of competing periodicities in PE was elucidated in [19].

Our experimental $T(E)$ data yield thus the energy positions, \mathbf{K}_{\parallel} dispersions and lifetimes of the PE final states. Apart from direct implications in the PE experiment such as tuning λ in energy and \mathbf{K}_{\parallel} , this information can be used as a vital input in computational simulations of the ME effects instrumental for resolving details of the valence $E(\mathbf{k})$ [2]. ME changes are expected between the $T(E)$ maxima owing to a phase change in the final-state wavefunction through the band gaps.

Intensities of diffracted beams: hidden c(2x2) periodicity and final-state diffraction effects – A typical normal-incidence VLEED image is shown in Fig.3 (left). Due to the IC superstructure the diffracted intensity is arranged in lines along ΓY [18,20], with non-vanishing intensity between the spots manifesting the fractal character of

diffraction in presence of two competing periodicities. The intense spots, each with IC satellites, are seen to reflect, firstly, the reciprocal lattice of the fundamental lattice at $(\pm 2\pi, 0)$ and $(0, \pm 2\pi)$. Surprisingly, there are other intense spots $(\pm\pi, \pm\pi)$ (arrows), although weaker in $(-\pi, \pi)$ and $(\pi, -\pi)$. Their symmetry reveals a hidden $c(2\times 2)$ periodicity. This phenomenon is observed in electron diffraction for the first time.

$I(V)$ data are shown in Fig.3 (*right*) as the VLEED intensity profile along an IC diffraction line, as a function of energy and $q_{(-\pi, \pi)}$ momentum transfer. All diffraction spots show a significant and non-monotonous energy dependence beyond the kinematic picture. The $c(2\times 2)$ spots are intense only below ~ 20 eV, and in the normal LEED energy range they vanish.

To identify the origin of the $c(2\times 2)$ periodicity, we first performed a kinematic simulation using the IC superstructure parameters from [21]. It has however yielded only the fundamental-lattice spots with IC satellites. Beyond the kinematic picture, possible origins of the $c(2\times 2)$ spots should be similar to the shadow FS with its $c(2\times 2)$ periodicity: either two inequivalent Cu sites per plane in the full orthorhombic unit cell of Bi2212 [6], or short-range AFM correlations within the CuO planes [5] manifesting themselves in VLEED through the exchange scattering [22]. However, the observed \mathbf{K}_{\parallel} broadening of both $c(2\times 2)$ spots and shadow FS seems too small compared to the short AFM correlation lengths found by neutron scattering. Finally, the $c(2\times 2)$ spots can be peaks of multiple scattering on the competing fundamental and IC potentials. Whichever the origin, the diffraction process involves multiple scattering between the CuO planes, and the outer SrO and BiO planes with their IC modulations [21]. The involvement of the CuO planes is corroborated the $c(2\times 2)$ intensity reduction with energy which goes along with the decrease of λ .

Complementing the information on the final states obtained from $T(E)$, the VLEED intensity distribution reflects their Fourier composition: Being the time-reversed LEED state, the final state can be expanded over the surface reciprocal vectors $\Phi(\mathbf{r}) = \sum_{\mathbf{g}} \phi_{\mathbf{g}}(r_{\perp}) e^{i(\mathbf{k}_{\parallel} + \mathbf{g})\mathbf{r}_{\parallel}}$, where the Fourier coefficients $\phi_{\mathbf{g}}(r_{\perp})$ correspond, in vacuum, to the incident and diffracted plane waves and, in the crystal, to the Bloch wavefield. The VLEED intensities $I_{\mathbf{g}}$ are the vacuum asymptotics of $|\phi_{\mathbf{g}}(r_{\perp})|^2$. As $\phi_{\mathbf{g}}(r_{\perp})$ run across the surface continuously in amplitude and derivative, $I_{\mathbf{g}}$ reflect, approximately, the Fourier composition of the final state in the crystal.

In the PE experiment this information immediately characterizes the final-state diffraction effects. For example, in the FS mapping experiment a \mathbf{g} -diffraction replica of the main FS occurs whenever upon variation of \mathbf{k}_{\parallel} the corresponding $\mathbf{k}_{\parallel} + \mathbf{g}$ Fourier component of the final state matches, in the parallel momentum, any Fourier component of the initial state, giving rise to non-zero overlap of

the final- and initial-state wavefunctions. The PE signal is then proportional, apart from phases of the Fourier components and selection rules entering the ME [1,2,7], to the final-state $|\phi_{\mathbf{g}}(r_{\perp})|^2$ and thus to its $I_{\mathbf{g}}$ asymptotics. Therefore, the PE signal of certain \mathbf{g} -diffraction replica follows, roughly, the \mathbf{g} -diffracted intensity observed in the VLEED image. The $I(V)$ data can then be used to tune the final-state energy to enhance or suppress certain diffraction replicas in the FS mapping experiment. Similar ideas can be exploited to single certain bands out of the valence band multitude based on their dominant Fourier component. Apart from Bi2212, such an approach can be applied to detail electronic structures of other complex materials, for example, perovskites.

Our VLEED data on the final-state diffraction effects leads to significant revisions in the current interpretation of some PE data on Bi2212. For example, the shadow FS with its $c(2\times 2)$ periodicity is commonly considered as an intrinsic effect pertinent to the initial state. To check against the extrinsic effects due to the final-state diffraction, we have measured VLEED images with incidence \mathbf{K}_{\parallel} set near the M point where a large shadow FS signal is found in the PE experiment. The $c(2\times 2)$ spots were found intense below ~ 25 eV and gradually vanishing at higher energies. This indicates that at low $h\nu$, commonly used in the PE experiment, the shadow FS intensity has a large extrinsic contribution. This is corroborated by the absence of a hybridization gap between the main and shadow FS [7]. The intrinsic shadow FS signal should be measured with higher $h\nu$ above 25 eV.

Finally, it should be noted that the final-state energies in PE, strictly speaking, differ from those observed in VLEED by the electron-hole interaction (excitonic) energy E_{e-h} . This figure, characterizing deviations from the sudden approximation, can be determined by comparing characteristic points in the PE intensity behavior with the predictions of VLEED. For typical layered materials such an analysis has however yielded negligible E_{e-h} values, at least on the scale of 100 meV [8].

Conclusion – Using VLEED with a support of full-potential band calculations, we have achieved first direct information on the energy positions, \mathbf{K}_{\parallel} dispersions, lifetimes and Fourier composition of the PE final states in Bi2212 at the excitation energies up to 45 eV above E_F . Implications of this information for the PE experiment extend from tuning λ to predictive use of the ME effects to focus on specific valence states or FS replicas. In particular, intense final-state $c(2\times 2)$ diffraction identifies significant extrinsic contribution to the shadow FS.

We thank M. Golden, A. Zakharov and E.E. Krasovskii for promoting discussions. The work was supported by Deutsche Forschungsgemeinschaft (grant Cl 124/5-1).

- [1] A. Bansil and M. Lindroos, Phys. Rev. Lett. **83**, 5154 (1999)
- [2] M. Lindroos, S. Sahrakorpi and A. Bansil, Phys. Rev. B **65**, 054514 (2002)
- [3] A.A. Kordyuk *et al*, Phys. Rev. Lett. **89**, 077003 (2002)
- [4] A. Damascelli, Z.-X. Shen and Z. Hussain, Rev. Mod. Phys., in press (2003)
- [5] P. Aebi *et al*, Phys. Rev. Lett. **72** (1994) 2757
- [6] H. Ding *et al*, Phys. Rev. Lett. **76** (1996) 1533
- [7] S.V. Borisenko *et al*, Phys. Rev. Lett. **84** (2000) 4453
- [8] V.N. Strocov *et al*, Phys. Rev. Lett. **79**, 467 (1997); J. Phys. Condens. Matter **10**, 5749 (1998)
- [9] V.N. Strocov *et al*, Phys. Rev. Lett. **81**, 4943 (1998); Phys. Rev. B **63**, 205108 (2001)
- [10] P. J. Feibelman and D. E. Eastman, Phys. Rev. B **10**, 4932 (1974)
- [11] E.E. Krasovkii *et al*, Phys. Rev. B **66**, 235403 (2002)
- [12] P. Blaha *et al*, WIEN2k, an augmented plane wave plus local orbitals program for calculating crystal properties. Vienna University of Technology, Austria, 2001
- [13] J.M. Tarascon *et al*, Phys. Rev. B **37**, 9382 (1988)
- [14] S.A. Sunshine *et al*, Phys. Rev. B **38**, 893 (1988)
- [15] V.N. Strocov, Solid State Commun. **106**, 101 (1997)
- [16] M.R. Norman *et al*, Phys. Rev. B **59**, 11191 (1999)
- [17] J.D. Lee and A. Fujimori, Phys. Rev. B **66**, 144509 (2002)
- [18] R. Claessen *et al*, Phys. Rev. B **39**, 7316 (1989)
- [19] J. Voit *et al*, Science **290**, 501 (2000)
- [20] P.A.P. Lindberg *et al*, Appl. Phys. Lett. **53** (1988) 2563
- [21] A. Yamamoto *et al*, Phys. Rev. B **42**, 4228 (1990)
- [22] P.W. Palmberg, R.E. DeWames and L.A. Vredevoe, Phys. Rev. Lett. **21** (1968) 682

FIG. 1. (a) Experimental $T(E)$ spectrum; (b) Structure in the experimental and calculated $T(E)$ enhanced by subtracting a quadratic background. The calculation is shifted by +3 eV to mimic $\Delta\Sigma$. The inset shows the experimental $\text{Im } \Sigma$ (with the uncertainty bars) compared with $\text{Im}[-1/\varepsilon]$; (c) Calculated $E(\mathbf{k})$ with the partial currents $T_{\mathbf{k}}$ shown by grayscale. The $T(E)$ maxima reflect manifolds of the final bands coupling to vacuum.

FIG. 2. Experimental \mathbf{K}_{\parallel} dispersion of the $T(E)$ spectra. The shading shows the energy regions of the $T(E)$ maxima, identified by $d^2T/dE^2 > 0$. The values of d^2T/dE^2 in these regions are represented in a logarithmic grayscale (black = maximal value). This map is the surface-projected dispersion of the PE final bands.

FIG. 3. (*left*) Normal-incidence VLEED image at an energy of 16.4 eV above E_F . The specular beam is in the center obscured by the electron gun. The diffracted intensity maxima reflect the fundamental lattice and a hidden $c(2\times 2)$ periodicity (arrows); (*right*) $I(V)$ data for the indicated IC diffraction line shown in a linear grayscale (white = maximal intensity). The coordinates on the LEED screen, somewhat distorted by the retarding field, are rendered into the $q_{(\pi, -\pi)}$ values.

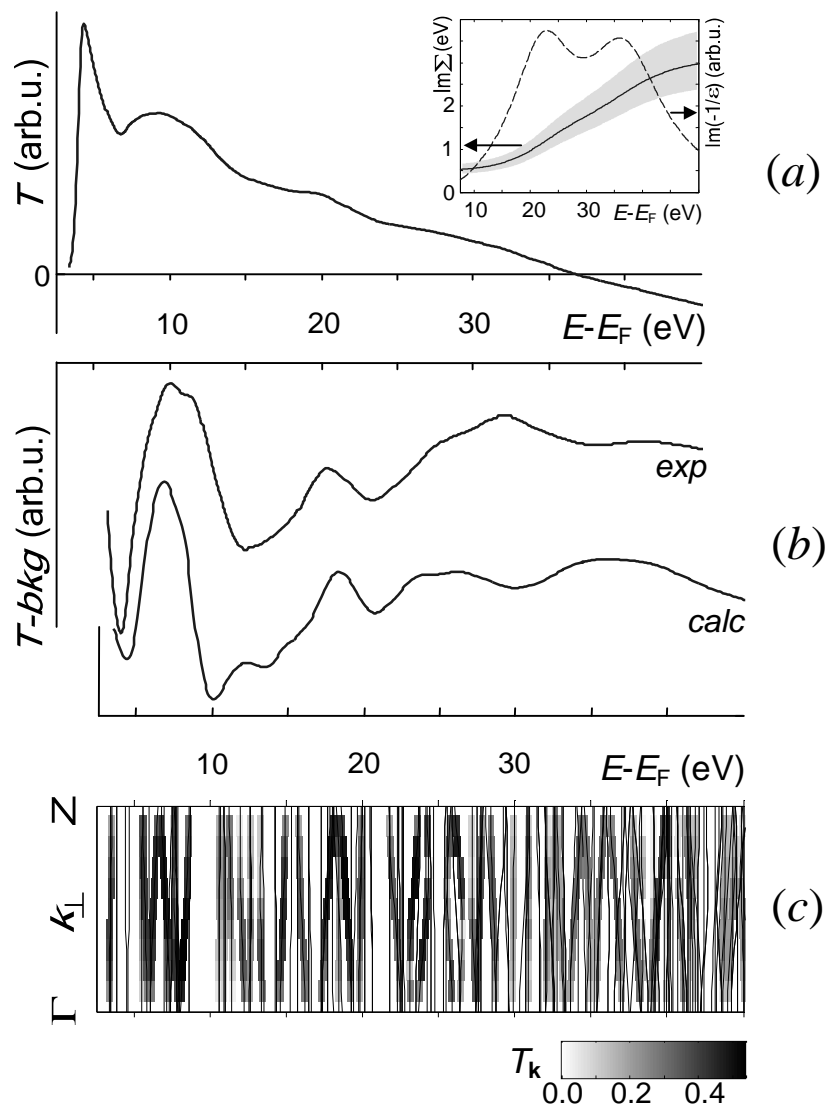


Fig.1 by Strocov *et al*

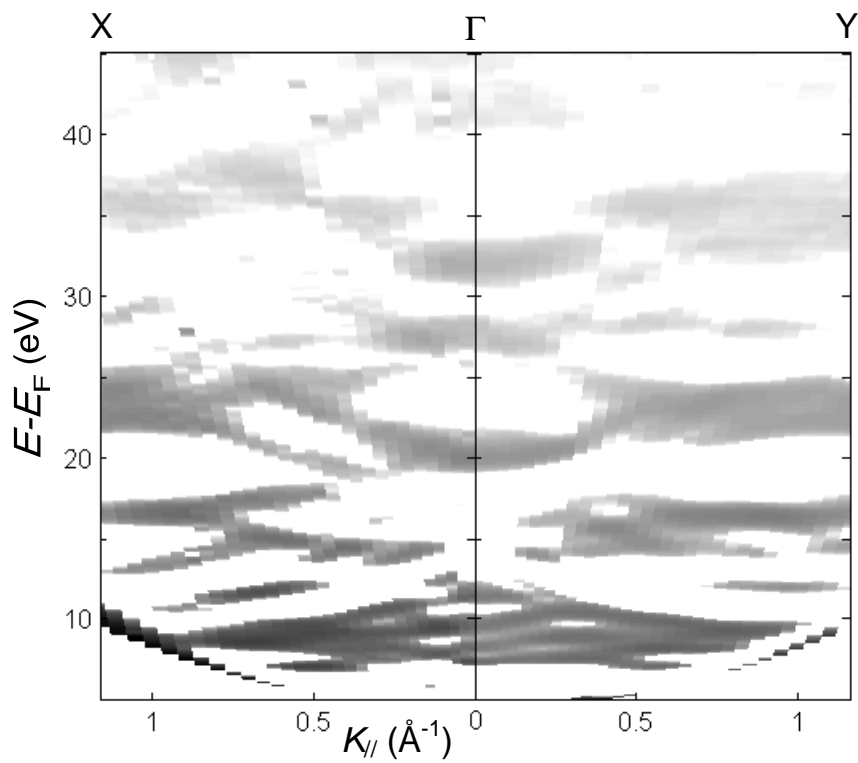


Fig.2 by Strocov *et al*

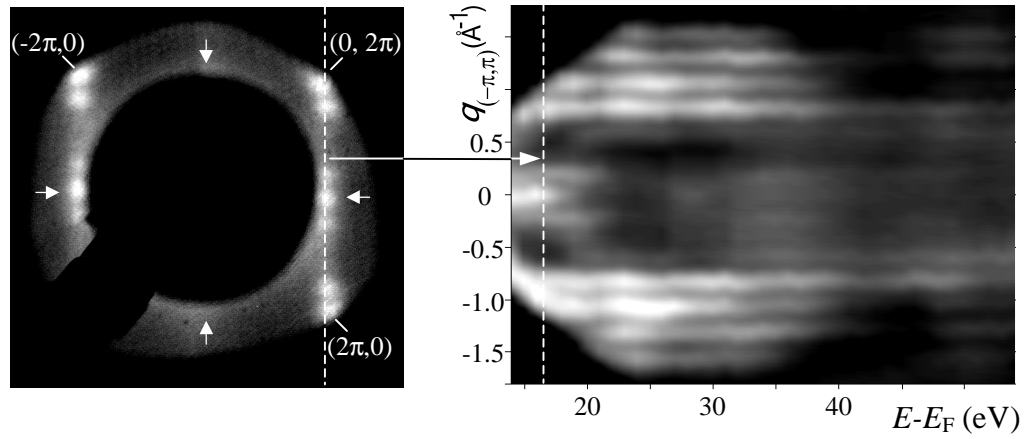


Fig.3 by Strocov *et al*